

pubs.acs.org/Macromolecules Article

Dilute Solution Properties of Poly(benzyl methacrylate) in Ionic Liquids

3 Aakriti Kharel, Cecilia Hall, Peter Černoch, Petr Stepanek, and Timothy P. Lodge*



Cite This: https://dx.doi.org/10.1021/acs.macromol.9b02618



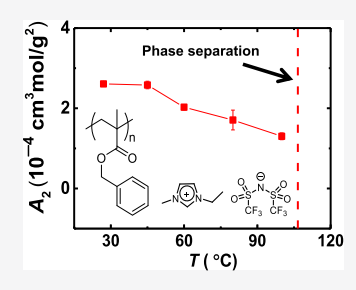
ACCESS

III Metrics & More

Article Recommendations

s Supporting Information

4 **ABSTRACT:** The static and dynamic properties of a range of molecular weights $(2 \times 10^4 \text{ to } 1.6 \times 10^5 \text{ g/mol})$ of poly(benzyl methacrylate) have been assessed in four different imidazolium- and 6 pyrrolidinium-based ionic liquids over a wide temperature range $(27-155 \, ^{\circ}\text{C})$, primarily using 7 light scattering techniques. All four systems exhibit lower critical solution temperature phase 8 behavior. The relevant structural, dynamic, and thermodynamic parameters were examined as a 9 function of concentration, temperature, and molecular weight. Some interesting observations were revealed. The phase boundaries suggest a shift of the critical composition toward the polymer-rich region, in contrast to the low critical concentrations for polymers commonly observed in polymer solutions. Surprisingly, the second virial coefficient (A_2) remains positive, even at temperatures 13 close to phase separation, where $A_2 < 0$ is anticipated. Furthermore, A_2 also shows stronger



dependence on molecular weight than commonly observed for polymers in good solvents. On the dynamic side, the diffusion virial scoefficients $(k_{\rm d})$ remained positive over the given temperature range, further corroborating the apparent good solvent behavior of A_2 . The excluded volume exponents $(\nu \approx 0.52-0.55)$ obtained from the dependence of hydrodynamic radii on molecular weight also indicate good solvent characteristics.

18 INTRODUCTION

19 Ionic liquids (ILs) are emerging as promising solvents for 20 polymers. 1-5 They exhibit excellent chemical and thermal 21 stability, favorable ionic conductivity, and negligible vapor 22 pressure, making them attractive alternatives to traditional 23 solvents. Moreover, adding polymers to ILs can provide 24 mechanical integrity to these materials while retaining their 25 transport properties, enabling their use in various applications 26 such as polymer electrolytes, gas separation membranes, and 27 energy storage. 6-12 However, the use of these materials would 28 benefit from a thorough understanding of polymer behavior in 29 ILs.

Among various combinations of polymers and ILs that could 30 31 be studied, poly(benzyl methacrylate) (PBzMA) in ILs is an 32 appealing candidate for two reasons. First, PBzMA in ILs 33 reveals interesting solution behavior, as demonstrated by 34 Watanabe and co-workers in recent years. 13-17 Of particular 35 interest is the lower critical solution temperature (LCST) 36 phase behavior of PBzMA in ILs that originates primarily from 37 the negative entropy of mixing ($\Delta S_{\text{mix}} < 0$). It has been 38 speculated that cation- π interactions between the imidazolium 39 cations and the aromatic rings in the PBzMA side chain result 40 in a structurally ordered solvation shell, lowering the entropy 41 of mixing. Watanabe and co-workers have reported the phase 42 transition (cloud point) temperatures (T_{cp}) of a fixed, low 43 concentration of PBzMA in a number of ILs. 13 Interestingly, 44 the values of $T_{\rm cp}$ were found to be significantly tunable with the 45 IL cation and anion identity, an observation that is similar to 46 polyethers and acrylates in ILs. $^{2,3,18-22}$ $T_{\rm cp}$ increased with the 47 increasing cation chain length for imidazolium cations

(C_n mim, where n = 1-8), spanning a temperature window 48 of almost 200 °C. On the other hand, changing the cation 49 structure from imidazolium to pyrrolidinium also increased 50 $T_{\rm cp}$, despite the absence of an aromatic ring in the latter. The 51 miscibility was reported to be remarkably sensitive to the 52 anions, as PBzMA only dissolved in bis-53 (trifluoromethylsulfonyl)imide (TFSI)-based and a few hexa- 54 fluorophosphate (PF₆)-based ILs. This interesting LCST-type 55 phase behavior motivates further study of the temperature- 56 dependent static and dynamic properties of PBzMA in ILs. 57 Second, the investigation of fundamental properties of PBzMA 58 in ILs is also advantageous from the application standpoint. In 59 the past decade, many advances have been made in utilizing 60 PBzMA and IL composites in thermosensitive applica- 61 tions.²³⁻²⁷ One such example is a thermoreversible ion gel 62 that can be obtained by the self-assembly of an ABA triblock, 63 with solvophobic block A and solvophilic block B.²⁷ PBzMA is 64 generally used as the A block, resulting in an ion gel that forms 65 on heating as the polymer becomes incompatible with the IL at 66 higher temperature because of its LCST behavior.

Light scattering is a powerful tool to elucidate the structure, 68 dynamics, and thermodynamics of polymer solutions. A few 69 light scattering studies have been reported for polymers in ILs. 70 Hoarfrost et al. reported a detailed investigation of polymer 71

Received: December 10, 2019 Revised: January 9, 2020



72 solution thermodynamics in ILs²¹ using a combination of 73 techniques—turbidimetry, static light scattering (SLS), and 74 small-angle neutron scattering (SANS)—at various temper-75 atures for poly(n-butyl methacrylate) (PnBMA) in mixtures of 76 1-ethyl-3-methylimidazolium bis(trifluoromethylsulfonyl)-77 imide ([EMIM][TFSI]) and 1-butyl-3-methylimidazolium 78 bis(trifluoromethylsulfonyl)imide ([BMIM] [TFSI]).²¹ Wata-79 nabe and co-workers used SANS to measure the second virial 80 coefficient (A_2) and evaluate the effective interaction 81 parameter $(\chi_{\rm eff})$ as a function of temperature for poly(N-82 isopropylacrylamide) (PNIPAm) and poly(2-phenylethyl 83 methacrylate) (PPhEtMA) in [EMIM][TFSI]. 17,28 The theta 84 temperatures are found to be 45 and 28 °C for PNIPAm and 85 PPhEtMA, respectively, where $A_2 = 0$ is obtained. For PBzMA 86 in IL, however, we are aware of only one work that has 87 reported an apparent R_g and hydrodynamic radius (R_h) change 88 with temperature near phase separation, using SANS and 89 dynamic light scattering (DLS). 14 This study reveals that two 90 populations (free polymer chains and aggregates) appear near 91 $T_{\rm cp}$. The effective interaction parameter $(\chi_{\rm eff})$ was also assessed 92 for a fixed concentration of PBzMA using SANS model fits. 93 The authors report χ_{eff} < 0.5, indicating that [EMIM][TFSI] is 94 a good solvent for PBzMA. However, the diffusion coefficients, 95 second virial coefficients, hydrodynamic radii, and their 96 dependence on concentration, polymer molecular weight, 97 and temperature are yet to be investigated.

This work describes the thermodynamic, dynamic, and 99 structural properties of a range of molecular weights of PBzMA 100 (20-160 kg/mol) in three different imidazolium-based ILs 101 and one pyrrolidinium-based IL, primarily using light 102 scattering techniques. The cloud point temperature is 103 evaluated by turbidimetry experiments to determine the 104 concentration dependence of $T_{\rm cp}$. Furthermore, $T_{\rm cp}$ is 105 measured as a function of the cation chain length and cation 106 identity. SLS is employed to evaluate A_2 for PBzMA, hence 107 establishing the molecular weight dependence of A_2 for these 108 systems. For the longest PBzMA chain, the temperature 109 dependence of A_2 is additionally examined over the range of 110 27-155 °C. DLS is used to measure the diffusivity as a 111 function of concentration and temperature (27–155 °C) to 112 evaluate the infinite dilution translation diffusion coefficient 113 (D_0) and the infinite dilution hydrodynamic radii $(R_{h,0})$. Flory 114 exponents (ν) are determined from the molecular weight 115 dependence of $R_{h,0}$. Additional relevant parameters such as the 116 diffusion virial coefficient (k_d) and frictional coefficient (k_f) are 117 determined from the concentration dependence of the mutual 118 diffusion coefficient, $D_{\rm m,}$ at several temperatures. Overall, the 119 key parameters of interest $(T_{\rm cp}, A_2, D_0, R_{\rm h,0}, \nu, k_{\rm d}, \text{ and } k_{\rm f})$ that 120 describe the behavior of dilute solutions of PBzMA in four ILs 121 are summarized and discussed.

EXPERIMENTAL SECTION

Polymer Synthesis and Characterization. All reagents were purchased from Sigma-Aldrich and used as received. In a representative ATRP protocol, benzyl methacrylate (10 g, 56.8 mmol), 1,1,4,7,10,10-hexamethyltriethylenetetramine (20 mg, 0.09 mmol), and ethyl-2-bromo-2-methylpropionate (7 mg, 0.09 mmol) were combined with anisole (284 mL) in a Schlenk flask. The mixture was degassed through three freeze—pump—thaw cycles and then placed under positive pressure of argon. A needle was placed in the septum to relieve pressure in the flask. The septum was removed from the reaction flask under a constant flow of argon, and copper(I) so bromide (6 mg, 0.04 mmol) was added. After re-sealing the flask and increasing the argon pressure to 5 atm, the reaction was allowed to

proceed at 75 °C for 3.5 h. The reaction mixture was quenched by 135 placing it in an ice water bath and purified by precipitation in hexanes 136 three times. The weight-average molecular weights $(M_{\rm w})$ and 137 dispersities (D) of the synthesized polymers (listed in Table 1) 138 t1

Table 1. Characteristics of PBzMA

$M_{\rm w}$ (kg/mol) ($\pm 10\%$) ^a	D^a	N^{b}	$c^* (g/mL)^c$
21	1.12	106	0.13
41	1.11	208	0.08
70	1.15	335	0.05
71 ^d	1.06	377	0.06
156	1.16	757	0.03

^aObtained from SEC (refractive index and light scattering detector) using THF as a mobile phase/. ^bCalculated using $M_{\rm n}/M_{\rm o}$, where $M_{\rm o}$ is the mass of repeat unit taken as 178 g/mol. ^cEstimated using $R_{\rm g}=0.011~M_{\rm w}^{0.588}$ (nm) for PBzMA in methyl ethyl ketone. ^dUsed for cloud point measurements.

were determined by size-exclusion chromatography (SEC) performed 139 in tetrahydrofuran (THF) at 25 °C on an Agilent 1260 Infinity 140 system. The eluents were monitored using a Wyatt Optilab T-rEX 141 refractive index detector (Figure S1), and the corresponding 142 molecular weights and distributions (summarized in Table 1) were 143 determined using Zimm plots obtained from a Wyatt Dawn Heleos II 144 multiangle laser light scattering detector, using a dn/dc of 0.144 mL/g 145 in THF. The polymers are denoted as PBzMA-x, where x denotes 146 the $M_{\rm w}$ of PBzMA, represented as PBzMA-20, PBzMA-40, PBzMA-147 70, and PBzMA-160 for 21, 41, 70, 156 kg/mol, respectively.

Sample Preparation. The ILs 1-ethyl-, 1-butyl-, and 1-hexyl-3- 149 methylimidazolium bis(trifluoromethyl-sulfonyl)imide ([EMIM]- 150 [TFSI], [BMIM][TFSI], [HMIM][TFSI], and 1-butyl-1-methyl- 151 pyrrolidinium TFSI [BMP][TFSI] were purchased from IoLiTec 152 and dried under dynamic vacuum (<100 mTorr) for 48 h at 60 °C. 153 The overlap concentrations (c^*) of PBzMA were estimated as $c^* = 154$ $3M/(4\pi R_g^3 N_A)$, where N_A is Avogadro's number and R_g is the radius 155 of gyration of PBzMA estimated using the relationship $R_{\rm g} = 0.011$ 156 $M_{\rm w}^{0.588}$ (nm) for PBzMA in methyl ethyl ketone (a good solvent).³⁰ 157 The values of c^* are listed in Table 1. In order to remain in the dilute 158 regime, all solutions were prepared with polymer concentrations 159 below c*. The polymer/IL solutions were prepared using co-solvent 160 evaporation as described elsewhere. 31 PBzMA and the IL were added 161 by weight in the desired ratio followed by the addition of THF to 162 facilitate dissolution. 13 THF was then evaporated under stirring using 163 a nitrogen purge overnight, and the mixtures were further dried under 164 vacuum (<100 mTorr) for 48 h at 60 °C. The solutions were carefully 165 filtered using a 0.45 μ m PTFE syringe filter into the sample cell for 166 scattering measurements. The concentrations in wt % were converted 167 into g/mL by using the appropriate density (assuming no change in 168 volume upon mixing) of the IL at each temperature. 32-34 The 169 temperature dependence of density (ρ) is estimated as $\rho = b - aT$, 170 where a and b are fitting parameters listed in Table S1 for all the ILs. 171

Cloud Point Measurements. PBzMA-71 solutions were flame- 172 sealed in glass ampoules under vacuum and placed in a heating stage 173 at a controlled temperature. The sample was heated at a rate of 1 °C/ 174 min, and a HeNe laser beam of wavelength 633 nm was directed to 175 the sample, with a path length of approximately 7 mm. The 176 transmitted intensity was recorded as a function of temperature, and 177 the cloud point was defined as the temperature at which the 178 transmittance drops to <80% of the original homogenous solution. 179 The cloud point temperature was recorded for an independent sample 180 (1 wt % PBzMA in [BMIM][TFSI]) upon heating and cooling at the 181 same rate. A relatively small hysteresis between demixing and 182 remixing was observed (see the Supporting Information, Figure S2) 183 with higher $T_{\rm cp}$ obtained upon cooling. Kobayashi et al. reported a 184 similar observation with PBzMA in solvate ILs. 15 They attributed the 185 hysteresis to the low mobility of polymer chains that dominated 186 remixing. For PBzMA in [BMIM][TFSI], the concentration range of 187 0.5-20 wt % was used to determine the concentration dependence of 188

189 $T_{\rm cp}$. Cloud point measurements were also performed for the highest 190 concentration of each molecular weight (see the Supporting 191 Information, Figure S3) and IL pair to decide the working 192 temperature range for SLS and DLS studies. The values of $T_{\rm cp}$ for 193 PBzMA-160 in [EMIM][TFSI], [BMIM][TFSI], [HMIM][TFSI], 194 and [BMP][TFSI] are 106 °C, 157 °C, 226 °C, and 176 °C, 195 respectively.

Static Light Scattering. Five different dilute concentrations for four molecular weights of PBzMA in four different ILs were prepared, 198 resulting in a total of 80 samples. The corresponding solutions (\sim 1 199 mL) were filtered into 12 mm glass ampoules and flame-sealed under 200 Ar. SLS measurements were performed on an ALV/CGS-8F 201 goniometer with a laser wavelength of 633 nm. The angular range 202 was $40-120^{\circ}$ in increments of 10° , corresponding to a scattering wave 203 vector (q) range of 9.42×10^{-3} to 2.44×10^{-2} nm⁻¹. In the given 204 angular range, no PBzMA exhibited any appreciable dependence on q 205 (see the Supporting Information, Figure S4), indicating that the 206 scattering falls in the Rayleigh regime ($qR_g \ll 1$). Therefore, the 207 values of second virial coefficients (A_2) were determined using the following expression

$$\frac{Kc}{R_{\theta}} = \frac{1}{M_{\rm W}} + 2A_{2}c + \dots \qquad K = \frac{4\pi^{2}n^{2}}{\lambda_{\rm o}^{4}N_{\rm A}} \left(\frac{\mathrm{d}n}{\mathrm{d}c}\right)^{2} \tag{1}$$

210 where R_{θ} is the Rayleigh ratio, K is an optical constant including the 211 solvent refractive index (n), and the wavelength of light in vacuum 212 (λ_{o}) . The measured Kc/R values were averaged over all the angles, 213 and plotted as a function of c to determine A_{2} from eq 1, as shown in 214 Figure 1 and the Supporting Information, Figure S5.

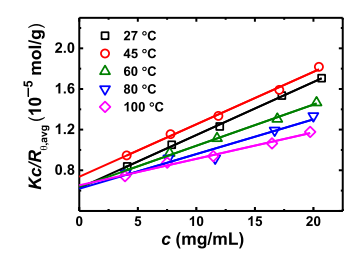


Figure 1. Representative plot of $Kc/R_{\theta,avg}$ as a function of c for PBzMA-160 in [EMIM][TFSI] at various temperatures.

For PBzMA-160, the measurements were performed at temperatures from 27 to 155 °C, maintained at \pm 0.5 °C. The samples were placed in a preheated sealed oven at the desired temperature before placing in the thermostated instrument for 5–10 min prior to the measurement. For T up to 130 °C, R_{θ} was calibrated using an 220 ultrapure toluene standard. For T > 130 °C (above the boiling 221 temperature of toluene in a sealed ampoule), R_{θ} was extrapolated 222 from the linear dependence of R_{θ} on T (see the Supporting 233 Information, Figure S6). The values of the refractive index (n) of the 224 ILs at each temperature were obtained from the literature. 36,37

For some systems at 27 °C, additional SLS measurements were performed on a Brookhaven BI-200SM research goniometer and laser light scattering system, with a laser wavelength of 637 nm. Scattering angles between 40 and 110° were used with 5° increments, corresponding to a q range of approximately 9.62×10^{-3} to 2.30×10^{-2} nm⁻¹. The Rayleigh ratio of the sample was calibrated using an ultrapure toluene standard at 27 °C. PBzMA and ILs solutions (~1 232 mL) were filtered into 13 mm glass tubes using 0.45 μ m PTFE filters and covered with parafilm. The samples were equilibrated for 10 min 234 at 27 °C prior to the measurement.

The refractive index increments were determined by Abbé refractometry. Five different solutions of PBzMA-40 were prepared in each IL, ranging in approximate concentration from 11 to 90 mg/ mL. The temperature in the refractometer was controlled by circulating water at 27 °C and 70:30 ethylene glycol/water bath at 240 45 and 60 °C. The refractive index $(n_{\rm D})$ of neat IL and five solutions were measured using a red light source to mimic the wavelength of

the laser in the light scattering instrument. Ideally, a wide temperature 242 window would be used for accurate extrapolation of dn/dc versus T, 243 but at higher temperatures, the measurement of $n_{\rm D}$ proved to be 244 unstable. Furthermore, dn/dc is very sensitive to slight changes in $n_{\rm D}$, 245 which makes the error in measuring dn/dc larger than the dependence 246 of dn/dc on T. Therefore, measurements were limited to 60 °C. 247

The dn/dc was evaluated from the slope of n_D versus c (see the 248 Supporting Information, Figure S7). The values of dn/dc for PBzMA 249 in ILs at three different temperatures are shown in Supporting 250 Information Figure S8, and listed in Table S2. The reported error is 251 obtained from linear fits of refractive index versus c. All systems show 252 a negligible temperature dependence for dn/dc within the uncertainty, 253 except for PBzMA in [BMIM][TFSI], which has a slight dependence 254 on T, $d(dn/dc)/dT = -1.1 \times 10^{-4}$ (mL/g °C). It is quite common to 255 observe a very weak dependence of dn/dc on T (typically on the order 256 of 10^{-4} mL/g °C) as reported in the literature. 21,38,39 For SLS 257 measurements above 60 °C, an average dn/dc value (measured at 3 258 temperatures) was used. On the other hand, for PBzMA in 259 [BMIM][TFSI], dn/dc at higher temperatures was calculated by 260 linear extrapolation.

Dynamic Light Scattering. DLS measurements were performed 262 on two different instruments. Measurements were conducted at 27 °C 263 on a Brookhaven BI-200SM research goniometer, laser light scattering 264 system, with a laser wavelength of 637 nm, and BI-9000AT 265 autocorrelator. Scattering angles of 30, 50, 70, 90, and 110° were 266 used corresponding to a q-range of 5.33×10^{-3} to 5.34×10^{-2} nm⁻¹ 267 and a typical acquisition time of 10 min per angle. The value of the 268 mean decay rate Γ was obtained from cumulant fitting of the intensity 269 autocorrelation function $|g^{(1)}|^2$ (see the Supporting Information, 270 Figure S9), and the size distribution was obtained via Laplace 271 inversion using REPES and the Stokes-Einstein equation (see the 272 Supporting Information, Figure S10). For the majority of the samples, 273 DLS measurements were performed on an ALV/CGS-8F goniometer 274 with a laser wavelength of 633 nm and an ALV 6010 correlator. The 275 angle was varied from 30 to 110° in increments of 20°, corresponding 276 to a q range of 5.34×10^{-3} to 5.35×10^{-2} nm⁻¹. For each angle, the 277 measurement was performed three times, averaged over 60 s each. 278 The value of Γ was also obtained from a third cumulant fit (see the 279 Supporting Information, Figure S9) determined by the inbuilt ALV 280 software, and the size distribution was obtained via Laplace inversion 281 using REPES and the Stokes-Einstein equation (see the Supporting 282 Information, Figure S10). Measurements at 27 °C for PBzMA-160 283 were made on both instruments for independent sets of samples with 284 equivalent concentrations. The values of D_0 obtained were generally 285 within 5% from the two independent measurements, emphasizing that 286 the collection time of 10 min versus 1 min does not significantly affect 287 the experimental values.

■ RESULTS AND DISCUSSION

Phase Behavior. As can be seen in Figure 2a, cloud point 290 f2 temperatures are obtained upon heating, consistent with the 291 known LCST phase behavior of PBzMA in ILs. 13 According to 292 the Flory-Huggins theory, particularly for UCST systems, the 293 critical concentration (ϕ_{c}) is generally shifted to low 294 concentrations of polymer and decreases with increasing 295 molecular weight ($\phi_{\rm c} \approx 1/N$, where N is the degree of 296 polymerization in units of solvent molar volume).⁴⁰ Using the 297 former relationship, ϕ_c is estimated to be 4 wt % for PBzMA- 298 71 (N = 393). However, as seen in Figure 2b, the observed 299 cloud point temperature decreases consistently up to at least 300 20 wt %, suggesting that the actual $\phi_{\rm c}$ may be far above the 301 estimated ϕ_c for PBzMA in [BMIM][TFSI]. Watanabe and co- 302 workers also conducted cloud point measurements for a similar 303 molecular weight of PBzMA in glyme-based ILs (equimolar 304 mixtures of triglyme (G3) or tetraglyme (G4) and LiTFSI, 305 resulting in Li(G3)TFSI and Li(G4)TFSI, respectively) and 306 observed a trend consistent with the results in Figure 2b. 16

289

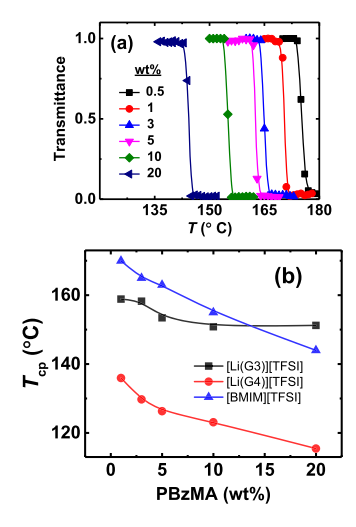


Figure 2. Cloud point measurements for PBzMA in ILs. (a) Transmittance vs temperature data for PBzMA (71 kg/mol) in [BMIM][TFSI] at a heating rate of 1 °C/min. (b) Cloud point temperature decreases continuously with increasing polymer concentration for PBzMA (71 kg/mol) in [BMIM][TFSI]. Watanabe and co-workers 15 measured cloud points for equivalent molecular weight PBzMA ($M_{\rm w}=70$ kg/mol, D=1.19) in glyme-based ILs (shown in red and black) and observed a similar trend. In all cases, the critical composition possibly lies far from the expected $\phi_{\rm c}$ of 4 wt %.

Although few full phase diagrams have been established for 309 polymers in ILs, some detailed work has been done for 310 polyethers in imidazolium-based ILs that also exhibit LCST 311 behavior. Unlike the PBzMA system, ϕ_c lies at low polymer 312 concentration ($\phi_{\rm c} \approx 4$ wt % for 22 kg/mol) for poly(ethyl 313 glycidyl ether) (PEGE) in [EMIM][TFSI].41 Furthermore, 314 this characteristic persists irrespective of the molecular weight 315 of PEGE. In contrast, poly(ethylene oxide) in [EMIM][BF₄] 316 and [BMIM][BF₄] exhibits unusually high ϕ_c (50–80 wt %), 317 similar to our observation for PBzMA in [BMIM][TFSI]. ^{19,20} 318 The origin of the higher critical composition is not fully 319 resolved in the PEO system but has been speculated to result 320 from the formation of dense polymer phases, as described by 321 de Gennes. 42 Recent theoretical work by Lipson and White has 322 provided two major explanations for occurrence of polymer-323 rich critical compositions in the PEO/[EMIM][BF₄] system. 43 324 First, the self-organization of IL molecules decreases their 325 contribution to the ideal entropy of mixing, as opposed to the 326 case if the solvent molecules were evenly distributed. Second, 327 the IL component has a significantly stronger cohesive energy 328 density compared to the polymer, which shifts the excess 329 entropy of mixing to higher polymer composition. These 330 arguments could partially explain the shift to higher polymer concentrations in our system as well. However, these explanations do not hold for the PEGE system, where the IL also has stronger cohesive energy density and the potential for self-organization. Therefore, the occurrence of higher critical compositions in these systems remains to be fully understood. Thermodynamic Properties. For PBzMA-160, the 337 temperature dependence of the second virial coefficient, A_2 , 338 is shown in Figure 3 in all the ILs, and the values are 339 summarized in Table 3. A2 decreases with increasing T, as 340 anticipated for an LCST system. However, A_2 remains 341 significantly positive even at temperatures close to the phase 342 separation temperature, $T_{\rm cp}$. The temperature at which $A_2=0$

343 (i.e., the theta temperature, T_{Θ}) is never reached in any of the

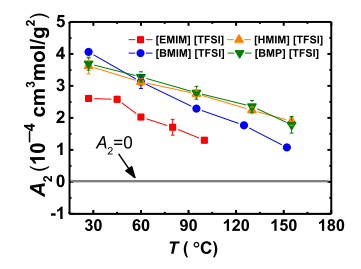


Figure 3. A_2 obtained from Zimm plots shown as a function of T. A_2 decreases with increasing T as anticipated for LCST systems. However, A_2 shows a weak dependence on T as the values of A_2 remain significantly positive even at T close to $T_{\rm cp}$. Solid lines are intended as guide to the eye.

Table 2. Entropic and Enthalpic Contributions to $\chi_{\rm eff}$

solvent	A	$B(K^{-1})$
[EMIM][TFSI]	0.64 ± 0.04	-73 ± 12
[BMIM][TFSI]	0.72 ± 0.01	-115 ± 5
[HMIM][TFSI]	0.55 ± 0.01	-65 ± 4
[BMP][TFSI]	0.58 ± 0.03	-72 ± 10

four ILs. This is particularly surprising for PBzMA in 344 [EMIM][TFSI] and [BMIM][TFSI], as the highest temper- 345 atures used are approximately $T_{\rm cp}-5$ °C, where $A_2<0$ is 346 anticipated. The consistently positive values of A_2 throughout 347 the temperature range imply that all these ILs are reasonably 348 good solvents in dilute solution. According to the Flory— 349 Huggins theory, the second virial coefficient can be related to 350 the interaction parameter, χ

$$A_2 = \left(\frac{1}{2} - \chi\right) \frac{\overline{V_2}^2}{\overline{V_1}} \frac{1}{M^2}$$
 (2) 352

where $\overline{V_2}$ is the partial molar volume of the polymer and $\overline{V_1}$ is 353 the partial molar volume of the solvent. Because χ typically has 354 an inverse dependence on T, A_2 is proportional to T^{-1} . 355 Therefore, A_2 is also plotted as a function of inverse T (see the 356 Supporting Information, Figure S11), which shows that the 357 experimentally obtained A_2 values are far from the $A_2 = 0$ line. 358 The major implication of this observation is that T_{Θ} is well 359 above $T_{\rm cp}$, an unusual characteristic, but one that is also 360 observed for hydroxypropylmethylcellulose in water. 44 For that 361 system, it was speculated that the solutions include some form 362 of aggregates that restrict the simple interpretation of A_2 . 363 However, for the PBzMA/IL system, DLS measurements at 364 various concentrations (~4-21 mg/mL) and temperatures 365 (27-100 °C) show no evidence of aggregation (see the 366 Supporting Information, Figure S10), particularly for PBzMA- 367 160 in [EMIM][TFSI] and [BMIM][TFSI], where the highest 368 measurement temperature is close to $T_{\rm cp}$.

Using eq 2 and the experimental values of A_2 , an effective 370 interaction parameter, $\chi_{\rm eff}$ can be evaluated at each temper- 371 ature. $\chi_{\rm eff}$ can be expressed as a function of temperature as $\chi_{\rm eff}$ 372 = A+B/T, where A represents the entropic contribution and B 373 includes the enthalpic contribution. In terms of the Flory- 374 Huggins theory, the excess entropy of mixing is equal to 375 $-kA\phi_p(1-\phi_p)$, and enthalpy of mixing is equal to $kB\phi_p(1-376)$ $kB\phi_p(1-376)$. The partial molar volume of the IL was used as the 377 reference volume, calculated using the density of the ILs at 378 each temperature. 32-34 The density of PBzMA was assumed to 379 vary insignificantly with temperature and, hence, a constant 380 value of 1.18 g/mL was used to estimate the partial molar 381

Table 3. Structural, Dynamic, and Thermodynamic Parameters of PBzMA-160 in ILs

r (°C)	$R_{\rm h,0}~(\rm nm)$	$D_0 \left(10^{-12} \text{ m}^2/\text{s} \right)$	$k_{\rm d}~({\rm mL/g})$	$A_2 (10^{-4} \text{ cm}^3 \text{ mol/g}^2)$	$k_{\rm f\; expt}\; ({\rm mL/g})$	$k_{\rm f\ theory}\ ({ m mL/g})$	$k_{ m f,expt}/k_{ m f,theor}$
PBzMA-	160 in [EMIM][[TFSI]					
27	8.3	0.90	8.7	2.61	73	58	1.3
45	8.0	1.73	5.2	2.58	75	57	1.3
60	7.9	2.68	5.4	2.03	58	46	1.3
80	7.1	4.40	4.2	1.71	49	38	1.3
100	5.9	6.55	1.0	1.30	39	28	1.4
PBzMA-	160 in [BMIM][[TFSI]					
27	8.3	0.58	10	4.06	116	85	1.4
60	8.1	2.06	8.8	3.13	89	67	1.3
95	7.9	4.95	9.2	2.29	62	51	1.2
125	7.4	9.00	5.4	1.77	50	40	1.3
152	6.5	14.9	0	1.08	34	25	1.4
PBzMA-	160 in [HMIM]	[TFSI]					
27	8.4	0.42	12	3.62	101	77	1.3
60	8.7	1.56	13	3.12	84	69	1.2
95	8.1	4.32	10	2.75	76	60	1.3
130	7.5	9.12	6.1	2.24	64	49	1.3
155	7.1	14.2	3.1	1.89	56	41	1.4
PBzMA-	160 in [BMP][T	TFSI]					
27	8.5	0.38	12	3.70	103	79	1.3
60	8.4	1.40	13	3.28	89	71	1.3
95	7.7	3.73	11	2.79	76	59	1.3
130	6.4	7.74	7.0	2.36	66	48	1.4
155	6.3	12.3	2.8	1.79	53	37	1.4

⁴⁵ volume of the polymer. The resulting dependence of χ_{eff} on temperature is shown in Figure 4, where χ_{eff} < 0.5 for all cases.

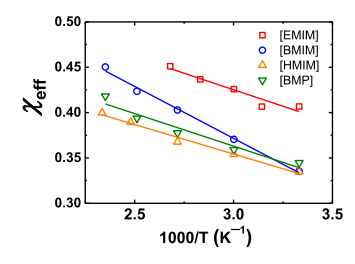


Figure 4. Temperature dependence of effective interaction parameter, χ_{eff} for PBzMA-160 in ILs. Solid lines are fit to $\chi_{\text{eff}} = A + B/T$, where A and B are fitting constants.

384 The values of A and B can be evaluated from the intercepts and 385 the slopes of the linear fits, respectively (listed in Table 2 and 386 plotted in the Supporting Information, Figure S12, with the 387 errors obtained from the linear fits). It should be emphasized 388 that the values of $\chi_{\rm eff}$, A, and B should all be viewed with 389 caution. For example, eq 2 does not incorporate any 390 composition dependence of $\chi_{\rm eff}$ therefore, the values of A 391 and B are not necessarily applicable at all compositions. 392 However, some prior reports have compared the values of A 393 and B to resolve the entropic and enthalpic components. 394 For example, Hoarfrost et al. showed that for PnBMA in 395 [EMIM][TFSI]/[BMIM][TFSI], 21 A increased with the 396 incorporation of the BMIM cation (75–100 wt %) and 397 concluded that the entropy of mixing decreases with higher 398 BMIM content. On the other hand, B decreased with 399 increasing BMIM content, which lowers the enthalpy of 400 mixing.

From Table 2, it can be seen that the values of *B* is negative in all cases, implying some kind of specific attractive interaction between the polymer and solvent. This result, combined with

the positive values of A, is indicative of LCST phase behavior. 404 Prior work by Watanabe and co-workers has proposed that the 405 benzyl groups in the polymer interact with the IL cation via 406 cation– π interactions, forming localized cage structures. ^{14,17,47} ₄₀₇ This interaction could be the primary driving force for the 408 negative enthalpy of mixing and decrease in entropy of mixing. 409 A recent study proposed that PBzMA solvation in IL is further 410 influenced by intrapolymer interactions between benzyl side 411 groups. 16 It can also be observed that the value of A increases 412 from EMIM to BMIM, indicating that the entropy of mixing 413 decreases. This observation is in agreement with prior reports, 414 where the incorporation of longer alkyl tails in the cations 415 decreased the mixing entropy because of oriented solvation. 21 416 However, this trend does not hold for the case when the 417 HMIM cation is used. In fact, the value of A decreases. On the 418 enthalpic side, the magnitude of B also exhibits a similar trend, 419 where |B| increases from EMIM to BMIM but decreases for 420 HMIM. Interestingly, the magnitude of A and B are very 421 similar for the EMIM and BMP cations. Therefore, no specific 422 trend can be concluded from these parameters. Hirosawa et al. 423 used SANS model fits to determine the parameters A and B for 424 a 40 kg/mol PBzMA in [EMIM][TFSI]. They report values of 425 A = 0.73 and B = -84 K⁻¹, which are close to the experimental 426 values obtained here.¹⁷

The Flory–Huggins theory predicts that A_2 is independent $_{428}$ of M (eq 2). In fact, A_2 is typically found to vary as $A_2 \approx M_w^a$, $_{429}$ where a is ≈ -0.2 for polymers in good solvents, as predicted $_{430}$ by the scaling theory $_{48-50}^{48-50}$ and reported in experiments. $_{51-54}^{51-54}$ $_{431}^{51}$ The A_2 values were also determined for the lower molecular $_{432}^{51}$ weight PBzMA samples at 27 °C (see the Supporting $_{433}^{51}$ Information, Figure S13), and the resulting values are shown $_{434}^{51}$ in Figure 5 for all systems and molecular weights. In all cases, $_{435}^{51}$ fs A_2 exhibits a stronger dependence on M_w than anticipated, $_{436}^{51}$ with a values of $_{51}^{51}$ or $_{52}^{51}$ or $_{52}^{51}$ or $_{53}^{51}$ or $_{54}^{51}$ or $_{54}^{$

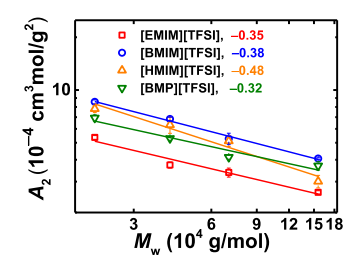


Figure 5. A_2 plotted as a function of $M_{\rm w}$ for PBzMA in ILs. A_2 decreases with increasing $M_{\rm w}$ as anticipated. $A_2 \approx M_{\rm w}{}^a$, where a is -0.35, -0.38, -0.48, and -0.32 for PBzMA in [EMIM][TFSI], [BMIM][TFSI], [HMIM][TFSI], and [BMP][TFSI], respectively. However, the dependence of A_2 on $M_{\rm w}$ is surprisingly stronger than observed for polymers in good solvent systems, where $a \approx -0.2$.

438 [EMIM][TFSI], [BMIM][TFSI], [HMIM][TFSI], and 439 [BMP][TFSI], respectively.

440 **Dynamic Properties.** The mutual diffusion coefficient 441 $(D_{\rm m})$ was determined from the slope of the mean decay rate Γ 442 plotted versus q^2 (see the Supporting Information, Figure S14) 443 for PBzMA-160 in all four ILs at 27 °C and $T_{\rm cp}-5$ °C. The 444 plots were linear for all cases. For all other temperatures 445 (between 27 °C and $T_{\rm cp}-5$ °C), DLS measurements were 446 performed only at a 90° scattering angle, where $D_{\rm m}$ was 447 evaluated as $D_{\rm m}=\Gamma/q^2$. The concentration dependence of the 448 mutual diffusion coefficient in dilute solutions can be 449 represented by

$$D_{\rm m} = D_0(1 + k_{\rm d}c + ...) \tag{3}$$

451 where D_0 is the infinite dilution translational diffusion 452 coefficient, c is the concentration, and the constant $k_{\rm d}$ is 453 known as the diffusion virial coefficient. ⁵⁴ $k_{\rm d}$ is given by

$$k_{\rm d} = 2A_2M - k_{\rm f} - V_{\rm p} \tag{4}$$

455 where $k_{\rm f}$ is the linear term in the concentration expansion for 456 the friction coefficient and $V_{\rm p}$ is the partial specific volume of 457 the polymer. The relations in eqs 3 and 4 contain both 458 thermodynamic and dynamic information. The coefficient $k_{\rm d}$ is 459 determined by the thermodynamic driving force $(2A_2M)$ and 460 an opposing frictional resistance, $k_{\rm f}$ (the contribution of $V_{\rm p}$ is 461 usually negligible). Positive values of $k_{\rm d}$ indicate good solvent 462 behavior, while in theta solvents, $k_{\rm d} \leq 0$.

The values of D_0 and $k_{\rm d}$ are summarized in Table 3 at all 464 temperatures and plotted in Figure 6 for PBzMA-160 in 465 [EMIM][TFSI] and in the Supporting Information, Figure 466 S15, for all other systems. $k_{\rm d}$ is also plotted as a function of 467 temperature for PBzMA-160 in all ILs in Figure 7. For 468 PBzMA-160 in [EMIM][TFSI], $k_{\rm d} > 0$ at $T_{\rm cp} - 5$ °C,

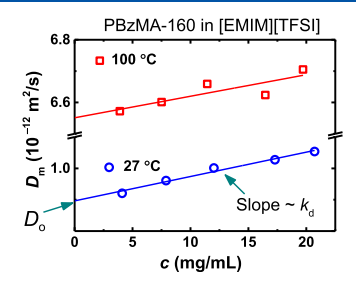


Figure 6. Representative plot of $D_{\rm m}$ vs c for PBzMA-160 in [EMIM][TFSI]. $D_{\rm m}$ varies linearly with c, and the slope and intercept of the linear fits give $k_{\rm d}$ and $D_{\rm o}$, respectively.

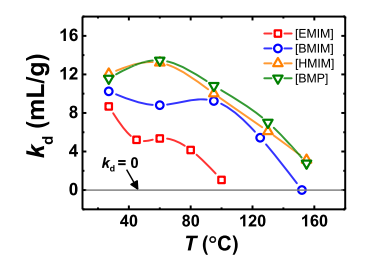


Figure 7. Temperature dependence of the diffusion virial coefficient for PBzMA-160 in ILs. The solid lines are the guide to the eye.

consistent with the good solvent behavior of the second virial 469 coefficient $(A_2>0)$ obtained from the Zimm plots. For 470 PBzMA in [BMIM][TFSI], $k_{\rm d}$ is essentially zero at $T_{\rm cp}$ –5 °C, 471 also indicating that A_2 is positive at $T_{\rm cp}$ –5 °C from eq 4. For 472 [HMIM][TFSI] and [BMP][TFSI], T=155 °C is far from 473 the observed $T_{\rm cp}$, and thus, the positive values of $k_{\rm d}$ are not 474 surprising. Overall, data from DLS further corroborate the 475 good solvent behavior of PBzMA in most of the ILs.

The frictional virial coefficient, $k_{\rm f}$ is estimated using the 477 measured experimental values of A_2 and $k_{\rm d}$ in eq 4 (assuming 478 $V_{\rm p}$ is negligible). Yamakawa 48 has established $k_{\rm f}$ as 479

$$k_{\rm f} \approx 1.2A_2M + N_{\rm A}\frac{V_{\rm m}}{M} \tag{5}$$

where $V_{\rm m}$ is the hydrodynamic volume of the polymer chain 481 and $N_{\rm A}$ is Avogadro's number. Accordingly, $k_{\rm f}$ was also 482 calculated using Yamakawa's approach. Here, the hydro- 483 dynamic volume is obtained by the relation, $V_{\rm m}=(4/3)\pi R_{\rm h}^{~3}$, 484 where $R_{\rm h}$ is obtained from the DLS measurements. From Table 485 3, it can be seen that the magnitude of calculated $k_{\rm f}$ is in 486 reasonable agreement with that estimated from the theory.

Based on the cloud point measurements and prior reports, 488 the miscibility of PBzMA-160 decreases with the cation type in 489 the following order: HMIM > BMP> BMIM > EMIM. In the 490 case of imidazolium-based cations, a similar conclusion may be 491 inferred from the A_2 and k_d values over the temperature range 492 of 27-100 °C (listed in Table 3 and shown in Figures 3 and 493 7). In particular, the values of A_2 are considerably lower for 494 PBzMA-160 in [EMIM][TFSI] compared to other ILs. This 495 observation is further supported by the $k_{
m d}$ values shown in 496 Figure 7. Overall, the combined results from the cloud point, 497 SLS, and DLS measurements support a consistent picture of 498 better solvation of PBzMA with increasing alkyl chain length of 499 the imidazolium cation. For PBzMA-160 in [BMP][TFSI], the 500 A_2 and k_d values are larger than those obtained in 501 [EMIM][TFSI] and [BMIM][TFSI], which is consistent 502 with the cloud point measurement. However, between BMP 503 and HMIM, no significant variation in A_2 and k_d was observed. 504 This suggests that the solvation properties of [BMP][TFSI] 505 are very similar to [HMIM][TFSI], a result that is particularly 506 surprising as the cloud point temperature is about 40 °C higher 507 in [HMIM][TFSI].

The concentration dependence of $D_{\rm m}$ was also measured for 509 the three lower molecular weights of PBzMA in all ILs at 27 °C 510 (see the Supporting Information, Figure S16). The values of $k_{\rm d}$ 511 and $D_{\rm 0}$ evaluated from the slopes and intercepts of the linear 512 fits of $D_{\rm m}$ versus. c plots, respectively, are listed in the 513 Supporting Information, Table S3 and plotted in the 514 Supporting Information, Figure S17. As seen in Table S3, $k_{\rm d}$ 515 remains positive for PBzMA-40 and PBzMA-70 but is negative 516 for all the cases of PBzMA-20. The negative values of $k_{\rm d}$ for 517

518 PBzMA-20 are not surprising as the A_2M term contribution is 519 smaller for lower molecular weight polymers in eq 4.

The infinite dilution hydrodynamic radii $(R_{\rm h,0})$ were calculated from the Stokes-Einstein relation

$$D_0 = \frac{kT}{6\pi\eta_s R_{h,0}} \tag{6}$$

523 where the solvent viscosity (η_s) was calculated using the 524 Vogel-Fulcher-Tamman (VFT) equation 32,34 given as $\eta_s = \eta_0$ 525 exp $(B/T - T_0)$ and η_0 , B, T_0 are fitting constants listed in 526 Table S4. 32,34 Figure 8 shows the temperature dependence of

522

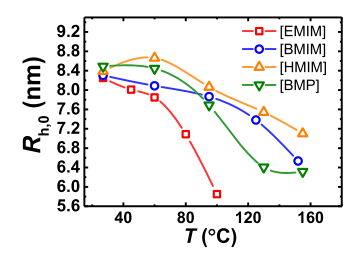


Figure 8. Temperature dependence of infinite dilution hydrodynamic radii for PBzMA-160 in ILs. The solid lines are the guide to the eye.

527 R_{h,0} for PBzMA-160 in all ILs, and the absolute values are 528 summarized in Table 4. For PBzMA-160 in [EMIM][TFSI],

Table 4. Hydrodynamic Radii and Scaling Exponents in Various ILs at 27 $^{\circ}\text{C}$

		$R_{\rm h,0}~({\rm nm})$				$R_{\rm h,0} = b \ M_{\rm w}^{\nu}$	
solvent	20k	40k	70k	160k	ν	b (nm)	
[EMIM][TFSI]	2.8	4.2	5.7	8.3	0.54	0.014	
[BMIM][TFSI]	2.9	4.3	5.9	8.3	0.53	0.014	
[HMIM][TFSI]	2.9	4.5	5.9	8.4	0.53	0.016	
[BMP][TFSI]	3.0	4.5	5.9	8.5	0.53	0.016	

529 [BMIM][TFSI], [HMIM][TFSI], and [BMP][TFSI], $R_{\rm h,0}$ 530 decreases by approximately 30, 21, 15, 26% over the 531 temperature range investigated, respectively. This behavior is 532 in agreement with other LCST systems, where solvent quality 533 worsens with increasing temperature, reducing the size of the 534 polymer chain.

The molecular weight dependence of both D_0 and $R_{\rm h,0}$ are safe shown in Table 4 and correspond to

$$R_{\rm h,0} = bM_{\rm w}^{\nu}$$

$$_{7} \qquad D_{0} \sim M_{\mathrm{w}}^{-\nu} \tag{7}$$

538 where ν is the Flory exponent and b is the prefactor. The 539 hydrodynamic radius is proportional to the radius of gyration, 540 where the proportionality factor is approximately 1.5 for 541 flexible polymer coils. The Because of this proportionality, $R_{\rm g,0}$ 542 and $R_{\rm h,0}$ follow the same dependence on $M_{\rm w}$ ($R_{\rm g} \approx R_{\rm h} \approx M^{\nu}$). The experimental values of ν along with the individual 544 hydrodynamic radii at 27 °C are listed in Table 4. The 545 exponents lie between 0.52 and 0.54, indicating that all ILs are 546 moderately good solvents for PBzMA at 27 °C. Consistent 547 with the Flory–Krigbaum theory, it is common to observe 548 values of ν between 0.5 and 0.6 because of the broad crossover 549 between Gaussian and swollen chain behavior. S9,60 It is also 550 possible that the values of ν would be higher if the dependence 551 of $R_{\rm p}$ on $M_{\rm w}$ were determined instead. The equilibrium

property, $R_{\rm gr}$ reflects solvent quality more directly than the 552 dynamic property, $R_{\rm h}$. As pointed out by des Cloizeaux⁶¹ and 553 further verified by Han and Akcasu,⁶² in practice, $R_{\rm h} \approx M^{\nu \prime}$ and 554 $R_{\rm g} \approx M^{\nu}$, $\nu' < \nu$, despite the expectation that $\nu' \approx \nu$ (Figure 9). 555 f9

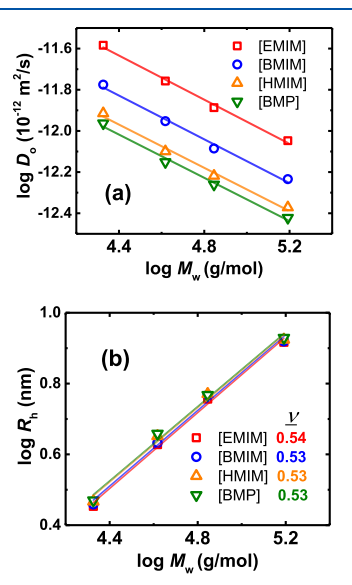


Figure 9. Infinite dilution dynamic properties of PBzMA in ILs at 27 °C. (a) Log D_0 varies linearly with log $M_{\rm w}$, where the slope yields $-\nu$. (b) $R_{\rm h,0}$ vs $M_{\rm w}$ also gives ν , where ν is between 0.52 and 0.54 for all solvents. Thus, the ILs are moderately good solvents for PBzMA at 27 °C

SUMMARY

The static and dynamic properties of a range of molecular 557 weights $(2 \times 10^4 \text{ to } 1.6 \times 10^5 \text{ g/mol})$ of PBzMA were assessed 558 in four different ILs using light scattering. The relevant 559 structural, dynamic, and thermodynamic parameters have been 560 examined as a function of concentration, temperature, and 561 molecular weight. The primary conclusions are as follows

- 1. Turbidimetry measurements reveal that the critical 563 concentration is shifted toward more polymer-rich 564 composition, as opposed to lower concentrations of 565 polymer anticipated by the original Flory—Huggins 566 theory. The phase separation temperatures increase 567 with increasing imidazolium-cation chain length and 568 changing the cation from imidazolium to pyrrolidinium, 569 consistent with prior reports.
- 2. Using SLS, second virial coefficients were obtained for 571 PBzMA-160 in the temperature range from 27 to 155 572 °C. A_2 is found to be consistently positive for all the 573 cases. This observation is particularly surprising for 574 PBzMA-160 in [EMIM][TFSI] and [BMIM][TFSI], as 575 the measurements were performed close to their phase 576 separation temperatures, where $A_2 < 0$ is anticipated. 577 The major implication of this result is that the theta 578 temperature $(A_2 = 0)$ lies above $T_{\rm cp}$, an unusual 579 behavior.
- 3. A_2 was also evaluated for other molecular weights of 581 PBzMA in all four ILs. It is found that A_2 exhibits a 582 stronger dependence on $M_{\rm w}$ ($A_2 \approx M_{\rm w}^{-0.3-0.5}$) in all 583 cases, compared to commonly observed dependence of 584 $A_2 \approx M_{\rm w}^{-0.2}$ for polymers in good solvents. 585

- 4. The mutual diffusion coefficients of PBzMA-160 in ILs were measured as a function of concentration at several temperatures (27–155 °C) using DLS. The $k_{\rm d}$ values obtained from the slopes of $D_{\rm m}$ vs c remain positive for almost all the cases, consistent with the positive values of A_2 obtained from the SLS measurements.
- 5. The frictional coefficients (k_f) calculated from the experimental A_2 and k_d values are in reasonable agreement with theoretical predictions.
- 6. $R_{\rm h,0}$ decreases approximately 15–30% with increasing T for PBzMA-160 as anticipated for an LCST system, where the solvent quality worsens with increasing T.
- 7. Flory exponents obtained from the $M_{\rm w}$ dependence of both D_0 and $R_{\rm h,0}$ lie between 0.52 and 0.54, indicating the ILs are moderately good solvents for PBzMA at 27 $^{\circ}C$

Overall, PBzMA in ILs, a representative LCST system, reveals some interesting solvation characteristics. The most that remarkable observation is that the thermodynamic and diffusion virial coefficients remain positive even in the proximity of phase separation. The presence of such unusual behavior in other polymer and ILs systems is an open question. We also present one of the first detailed sets of thermodynamic and dynamic parameters for a polymer and IL system using light scattering, which lays the groundwork for future studies to investigate more relevant polymers and ILs mixtures that are tize viable in light scattering.

613 **ASSOCIATED CONTENT**

614 Supporting Information

586

587

588

589

590

591

592

593

594

595

596

597

598

599

600

615 The Supporting Information is available free of charge at 616 https://pubs.acs.org/doi/10.1021/acs.macromol.9b02618.

SEC traces, light scattering data, refractive index data, DLS correlation functions, fitting, and diffusion characteristics (PDF)

620 AUTHOR INFORMATION

621 Corresponding Author

Timothy P. Lodge — University of Minnesota,
Minneapolis, Minnesota; orcid.org/0000-0001-59168834; Email: lodge@umn.edu

625 Other Authors

Aakriti Kharel – University of Minnesota, Minneapolis,
Minnesota

628 **Cecilia Hall** – University of Minnesota, Minneapolis, Minnesota; © orcid.org/0000-0003-2773-1279

Peter Černoch – Czech Academy of Sciences, Prague, Czech Republic

Petr Stepanek – Czech Academy of Sciences, Prague, Czech Republic; o orcid.org/0000-0003-1433-678X

634 Complete contact information is available at:

635 https://pubs.acs.org/10.1021/acs.macromol.9b02618

636 Notes

637 The authors declare no competing financial interest.

38 ACKNOWLEDGMENTS

639 This work was supported by the National Science Foundation 640 (DMR-1707578), the Grant agency of the Czech Republic 641 (grant 19-10429S), and the Ministry of Education, Youth and

Sports of CR within the National Sustainability Program I 642 (NPU I), Project POLYMAT LO1507. Helpful discussions 643 with Dr. Svetlana Morozova are appreciated.

REFERENCES

(1) Lodge, T. P. MATERIALS SCIENCE: A Unique Platform for 646 Materials Design. *Science* **2008**, 321, 50–51.

645

- (2) Ueki, T.; Watanabe, M. Polymer in ionic liquids: dawn of 648 neoteric solvents and innovative materials. *Bull. Chem. Soc. Jpn.* **2012**, 649 85, 33–50.
- (3) Ueki, T.; Watanabe, M. Macromolecules in ionic liquids: 651 progress, challenges, and opportunities. *Macromolecules* **2008**, 41, 652 3739–3749.
- (4) Xie, H.; Li, S.; Zhang, S. Ionic liquids as novel solvents for the 654 dissolution and blending of wool keratin fibers. *Green Chem.* **2005**, *7*, 655 606–608.
- (5) Winterton, N. Solubilization of polymers by ionic liquids. J. 657 Mater. Chem. 2006, 16, 4281–4293.
- (6) Sato, T.; Masuda, G.; Takagi, K. Electrochemical properties of 659 novel ionic liquids for electric double layer capacitor applications. 660 *Electrochim. Acta* **2004**, 49, 3603–3611.
- (7) Choi, J.-H.; Xie, W.; Gu, Y.; Frisbie, C. D.; Lodge, T. P. Single 662 ion conducting, polymerized ionic liquid triblock copolymer films: 663 high capacitance electrolyte gates for n-type transistors. ACS Appl. 664 Mater. Interfaces 2015, 7, 7294–7302.
- (8) Mecerreyes, D. Polymeric ionic liquids: broadening the 666 properties and applications of polyelectrolytes. *Prog. Polym. Sci.* 667 **2011**, 36, 1629–1648.
- (9) Gu, Y.; Lodge, T. P. Synthesis and gas separation performance of 669 triblock copolymer ion gels with a polymerized ionic liquid mid-block. 670 *Macromolecules* **2011**, 44, 1732–1736.
- (10) Chopade, S. A.; So, S.; Hillmyer, M. A.; Lodge, T. P. 672 Anhydrous proton conducting polymer electrolyte membranes via 673 polymerization-induced microphase separation. *ACS Appl. Mater.* 674 Interfaces 2016, 8, 6200–6210.
- (11) Chopade, S. A.; Au, J. G.; Li, Z.; Schmidt, P. W.; Hillmyer, M. 676 A.; Lodge, T. P. Robust polymer electrolyte membranes with high 677 ambient-temperature lithium-ion conductivity via polymerization- 678 induced microphase separation. ACS Appl. Mater. Interfaces 2017, 9, 679 14561–14565.
- (12) Osada, I.; de Vries, H.; Scrosati, B.; Passerini, S. Ionic-liquid- 681 based polymer electrolytes for battery applications. *Angew. Chem., Int.* 682 *Ed.* **2016**, *55*, 500–513.
- (13) Ueki, T.; Arai, A. A.; Kodama, K.; Kaino, S.; Takada, N.; 684 Morita, T.; Nishikawa, K.; Watanabe, M. Thermodynamic study on 685 phase transitions of poly(benzyl methacrylate) in ionic liquid solvents. 686 *Pure Appl. Chem.* **2009**, *81*, 1829–1841.
- (14) Fujii, K.; Ueki, T.; Niitsuma, K.; Matsunaga, T.; Watanabe, M.; 688 Shibayama, M. Structural aspects of the LCST phase behavior of 689 poly(benzyl methacrylate) in room-temperature ionic liquid. *Polymer* 690 **2011**, 52, 1589–1595.
- (15) Kobayashi, Y.; Kitazawa, Y.; Hashimoto, K.; Ueki, T.; Kokubo, 692 H.; Watanabe, M. Thermosensitive phase separation behavior of 693 poly(benzyl methacrylate)/solvate ionic liquid solutions. *Langmuir* 694 **2017**, 33, 14105–14114.
- (16) Fujii, K.; Ueki, T.; Hashimoto, K.; Kobayashi, Y.; Kitazawa, Y.; 696 Hirosawa, K.; Matsugami, M.; Ohara, K.; Watanabe, M.; Shibayama, 697 M. Microscopic structure of solvated poly(benzyl methacrylate) in an 698 imidazolium-based ionic liquid: high-energy X-ray total scattering and 699 all-atom MD simulation study. *Macromolecules* **2017**, 50, 4780–4786. 700
- (17) Hirosawa, K.; Fujii, K.; Ueki, T.; Kitazawa, Y.; Littrell, K. C.; 701 Watanabe, M.; Shibayama, M. SANS study on the solvated structure 702 and molecular interactions of a thermo-responsive polymer in a room 703 temperature ionic liquid. *Phys. Chem. Chem. Phys.* **2016**, *18*, 17881–704 17889.
- (18) Kodama, K.; Tsuda, R.; Niitsuma, K.; Tamura, T.; Ueki, T.; 706 Kokubo, H.; Watanabe, M. Structural effects of polyethers and ionic 707

- ₇₀₈ liquids in their binary mixtures on lower critical solution temperature ₇₀₉ liquid-liquid phase separation. *Polym. J.* **2011**, *43*, 242–248.
- 710 (19) Lee, H.-N.; Lodge, T. P. Lower critical solution temperature 711 (LCST) phase behavior of poly(ethylene oxide) in ionic liquids. *J.* 712 *Phys. Chem. Lett.* **2010**, *1*, 1962–1966.
- 713 (20) Lee, H.-N.; Newell, N.; Bai, Z.; Lodge, T. P. Unusual lower 714 critical solution temperature phase behavior of poly(ethylene oxide) 715 in ionic liquids. *Macromolecules* **2012**, *45*, 3627–3633.
- 716 (21) Hoarfrost, M. L.; He, Y.; Lodge, T. P. Lower critical solution 717 temperature phase behavior of poly(n-butyl methacrylate) in ionic 718 liquid mixtures. *Macromolecules* **2013**, *46*, 9464–9472.
- 719 (22) Kharel, A.; Lodge, T. P. Effect of ionic liquid components on 720 the coil dimensions of PEO. *Macromolecules* **2019**, *52*, 3123–3130.
- 721 (23) Lodge, T. P.; Ueki, T. Mechanically tunable, readily processable 722 ion gels by self-assembly of block copolymers in ionic liquids. *Acc.* 723 *Chem. Res.* **2016**, *49*, 2107–2114.
- 724 (24) Ueki, T. Stimuli-responsive polymers in ionic liquids. *Polym. J.* 725 **2014**, 46, 1-10.
- 726 (25) Lee, H.-N.; Bai, Z.; Newell, N.; Lodge, T. P. Micelle/inverse 727 micelle self-assembly of a peo-pnipam block copolymer in ionic 728 liquids with double thermoresponsivity. *Macromolecules* **2010**, 43, 729 9522–9528.
- 730 (26) Hall, C. C.; Lodge, T. P. Photoreversible order-disorder 731 transition in an ionic liquid solvated block polymer. *ACS Macro Lett.* 732 **2019**, *8*, 393–398.
- 733 (27) Kitazawa, Y.; Ueki, T.; Niitsuma, K.; Imaizumi, S.; Lodge, T. P.; 734 Watanabe, M. Thermoreversible high-temperature gelation of an ionic 735 liquid with poly(benzyl methacrylate-b-methylmethacrylate-b-benzyl-736 methacrylate) triblock copolymer. *Soft Matter* **2012**, *8*, 8067–8074.
- 736 methactylate) tholock copolymer. *Soft Matter* **2012**, *8*, 8067–8074.
 737 (28) Asai, H.; Fujii, K.; Ueki, T.; Sawamura, S.; Nakamura, Y.;
 738 Kitazawa, Y.; Watanabe, M.; Han, Y.-S.; Kim, T.-H.; Shibayama, M.
 739 Structural study on the ucst-type phase separation of poly(N
 740 -isopropylacrylamide) in ionic liquid. *Macromolecules* **2013**, *46*,
 741 1101–1106.
- 742 (29) Podzimek, S. Light Scattering, Size Exclusion Chromatography 743 and Asymmetric Flow Field Flow Fractionation: Powerful Tools for the 744 Characterization of Polymers, Proteins and Nanoparticles; John Wiley & 745 Sons: New Jersey, 2011.
- 746 (30) Richards, R. W. Dilute solution properties of poly(benzyl 747 methacrylate). *Polymer* **1977**, *18*, 114–120.
- 748 (31) Kharel, A.; Lodge, T. P. Coil dimensions of poly(ethylene 749 oxide) in an ionic liquid by small-angle neutron scattering. 750 *Macromolecules* **2017**, *50*, 8739—8744.
- 751 (32) Tokuda, H.; Hayamizu, K.; Ishii, K.; Susan, M. A. B. H.; 752 Watanabe, M. Physicochemical properties and structures of room 753 temperature ionic liquids. 2. Variation of alkyl chain length in 754 imidazolium cation. *J. Phys. Chem. B* **2005**, *109*, 6103–6110.
- 755 (33) Tokuda, H.; Hayamizu, K.; Ishii, K.; Susan, M. A. B. H.; 756 Watanabe, M. Physicochemical properties and structures of room 757 temperature ionic liquids. 1. Variation of anionic species. *J. Phys.* 758 *Chem. B* **2004**, *108*, 16593–16600.
- 759 (34) Tokuda, H.; Ishii, K.; Susan, M. A. B. H.; Tsuzuki, S.; 760 Hayamizu, K.; Watanabe, M. Physicochemical properties and 761 structures of room-temperature ionic liquids. 3. Variation of cationic 762 structures. *J. Phys. Chem. B* **2006**, *110*, 2833–2839.
- 763 (35) Lodge, T. P.; Hiemenz, P. C. Polymer Chemistry, 2nd ed.; CRC 764 Press, 2007.
- 765 (36) Montalbán, M. G.; Bolívar, C. L.; Díaz Baños, F. G.; Víllora, G. 766 Effect of temperature, anion, and alkyl chain length on the density and 767 refractive index of 1-alkyl-3-methylimidazolium-based ionic liquids. *J. 768 Chem. Eng. Data* **2015**, *60*, 1986–1996.
- 769 (37) Seoane, R. G.; Corderí, S.; Gómez, E.; Calvar, N.; González, E. 770 J.; MacEdo, E. A.; Domínguez, Á. Temperature dependence and 771 structural influence on the thermophysical properties of eleven 772 commercial ionic liquids. *Ind. Eng. Chem. Res.* 2012, 51, 2492–2504. 773 (38) Horská, J.; Stejskal, J.; Kratochvíl, P. Refractive index 774 increments of polyethylene. *J. Appl. Polym. Sci.* 1979, 24, 1845–1855.

- (39) Chiang, R.; Carolina, N. The temperature dependence of the 775 specific refractive index increment of polyethylene in various solvents. 776 *J. Polym. Sci., Part C: Polym. Symp.* 1965, 304, 295–304.
- (40) Flory, P. J. Principles of Polymer Chemistry; Cornell University 778 Press: New York, 1953.
- (41) Tsuda, R.; Kodama, K.; Ueki, T.; Kokubo, H.; Imabayashi, S.-i.; 780 Watanabe, M. LCST-type liquid-liquid phase separation behaviour of 781 poly(ethylene oxide) derivatives in an ionic liquid. *Chem. Commun.* 782 **2008**, 4939–4941.
- (42) de Gennes, P. G. Special features of water soluble polymers. 784 Pure Appl. Chem. 1992, 64, 1585–1588.
- (43) White, R. P.; Lipson, J. E. G. Origins of unusual phase behavior 786 in polymer/ionic liquid solutions. *Macromolecules* **2013**, 46, 5714–787 5723.
- (44) Lodge, T. P.; Maxwell, A. L.; Lott, J. R.; Schmidt, P. W.; 789 McAllister, J. W.; Morozova, S.; Bates, F. S.; Li, Y.; Sammler, R. L. 790 Gelation, phase separation, and fibril formation in aqueous 791 hydroxypropylmethylcellulose solutions. *Biomacromolecules* **2018**, *19*, 792 816–824.
- (45) Mandal, T. K.; Kuo, J. F.; Woo, E. M. Miscibility and spherulite 794 growth kinetics in the poly(ethylene oxide)/poly(benzyl methacry-795 late) system. *J. Polym. Sci., Part B: Polym. Phys.* **2000**, 38, 562–572. 796
- (46) Scholte, T. G. Determination of thermodynamic parameters of 797 polymer-solvent systems by light scattering. *European Polymer Journal* 798 **1970**, *6*, 1063–1074.
- (47) Ueki, T.; Watanabe, M. Lower critical solution temperature 800 behavior of linear polymers in ionic liquids and the corresponding 801 volume phase transition of polymer gels. *Langmuir* **2007**, 23, 988–802 990.
- (48) Yamakawa, H. Modern Theory of Polymer Solutions; Harper and 804 Row: New York, 1971.
- (49) de Gennes, P.-G. Scaling Concepts in Polymer Physics; Cornell 806 University Press: New York, 1979.
- (50) des Cloizeaux, J. Polymers in Solution; Clarendon Press: Oxford, 808
- (51) Sung, J. H.; Lee, D. C.; Park, H. J. Conformational 810 characteristics of poly(ethylene oxide) (PEO) in methanol. *Polymer* 811 **2007**, 48, 4205–4212.
- (52) Fetters, L. J.; Hadjichristidis, N.; Lindner, J. S.; Mays, J. W. 813 Molecular weight dependence of hydrodynamic and thermodynamic 814 properties for well-defined linear polymers in solution. *J. Phys. Chem.* 815 *Ref. Data* 1994, 23, 619–640.
- (53) Kinugasa, S.; Nakahara, H.; Kawahara, J.-I.; Koga, Y.; Takaya, 817 H. Static light scattering from poly(ethylene oxide) in methanol. *J.* 818 *Polym. Sci., Part B: Polym. Phys.* **1996**, 34, 583–586.
- (54) Devanand, K.; Selser, J. C. Asymptotic behavior and long-range 820 interactions in aqueous solutions of poly(ethylene oxide). *Macro-molecules* **1991**, *24*, 5943–5947.
- (55) Bhatt, M.; Jamieson, A. M.; Petschek, R. G. Static and dynamic 823 scaling relationships in the light scattering properties of polystyrenes 824 in good solvents. *Macromolecules* **1989**, 22, 1374–1380. 825
- (\$\sigma 6\$) Bhatt, M.; Jamieson, A. M. Dynamic light scattering studies of 826 polystyrene in tetrahydrofuran at intermediate scattering vectors. 827 *Macromolecules* **1988**, 21, 3015–3022. 828
- (57) Wu, C.; Wang, X. Globule-to-coil transition of a single 829 homopolymer chain in solution. *Phys. Rev. Lett.* **1998**, 80, 4092–4094. 830 (58) De Gennes, P. G. Dynamics of entangled polymer solutions. ii. 831 inclusion of hydrodynamic interactions. *Macromolecules* **1976**, *9*, 832
- (59) Flory, P. J.; Krigbaum, W. R. Statistical mechanics of dilute 834 polymer solutions. II. *J. Chem. Phys.* **1950**, *18*, 1086.
- (60) Krigbaum, W. R.; Flory, P. J. Statistical Mechanics of Dilute 836 Polymer Solutions. IV. Variation of the Osmotic Second Coefficient 837 with Molecular Weight1a, b. *J. Am. Chem. Soc.* **1953**, 75, 1775–1784. 838 (61) Weill, G.; des Cloizeaux, J. Dynamics of polymers in dilute 839
- solutions: an explanation of anomalous indices by cross-over effects. *J.* 840 *Phys.* **1979**, *40*, 99–105.

https://dx.doi.org/10.1021/acs.macromol.9b02618 *Macromolecules* XXXX, XXX, XXX–XXX

594-598.

842 (62) Akcasu, A. Z.; Han, C. C. Molecular weight and temperature 843 dependence of polymer dimensions in solution. *Macromolecules* **1979**, 844 *12*, 276–280.